Chemical Science

ROYAL SOCIETY OF CHEMISTRY

EDGE ARTICLE

View Article Online
View Journal

Cite this: DOI: 10.1039/d5sc08977h

All publication charges for this article have been paid for by the Royal Society of Chemistry

Received 17th November 2025
Accepted 30th December 2025

DOI: 10.1039/d5sc08977h

rsc.li/chemical-science

Cation radical-mediated semi-pinacol and *n*+2 ring expansions *via* organic photoredox catalysis

Brandon B. Fulton,† Connor T. Owen † and David A. Nicewicz *

In this report, we disclose a photoredox-catalyzed cation radical-mediated semi-pinacol (CRM-SP) rearrangement along with a similar, but mechanistically distinct, *n*+2 ring expansion with protocols for obtaining either dearomatized or rearomatized products. We present a substrate scope of >30 entries largely focused on the ring expansion of easily appended cyclobutanols and targeting medicinally relevant scaffolds, highlighting the utilization of the methodology for diversification. Gram scale reactions in batch and continuous flow were investigated. Additionally, the mechanism is probed both experimentally and computationally with results suggesting a substrate-dependent set of pathways featuring either (A) a concerted 1,2-shift or (B) a sequence of proton-coupled electron transfer (PCET), β-scission, Giese addition, and terminal hydrogen atom transfer (HAT).

Introduction

Rearrangement reactions are an indispensable tool in organic synthesis, paralleled by few in their ability to rapidly transform simple intermediates into complex molecular frameworks. A thoughtfully designed rearrangement-based synthetic strategy can streamline the transmutation of inexpensive and accessible starting materials into difficult-to-access scaffolds with high synthetic efficiency, often featuring non-intuitive skeletal reorganizations. This relationship between efficiency and complexity has made rearrangement reactions particularly attractive in the field of natural product total synthesis, where minimizing synthetic effort to access chemical space of ever-increasing sophistication is of paramount importance.[1] While ionic rearrangements – especially those involving cations – have been extensively studied, their radical analogues have only recently received considerable attention with the advent of modern enabling technologies such as photoredox catalysis and the concurrent development of modalities for increased control of radical species.[2,3] Even less studied are rearrangement reactions in which charged radical species such as cation and anion radicals directly participate in, or are used as initiators for, skeletal reorganizations.[4–13]

In an effort to expand the arsenal of transformations enabled by organic photoredox catalysis, our group sought to probe the ability of cation radicals to serve as migratory acceptors in rearrangement reactions. Our initial conceptualization of this transformation is shown in Scheme 1a, in which a cation radical could first be generated *via* single-electron transfer (SET) oxidation of an alkene-containing substrate by a photocatalyst. This electron hole, when placed strategically adjacent to a tertiary alcohol featuring a substituent of high migratory aptitude, could then induce a semi-pinacol-like rearrangement through C=O double bond formation concomitant with a 1,2-shift of the migrating group. This transformation is notably distinct from traditional semi-pinacol type rearrangements in that there is no classical leaving group, bearing more resemblance to protio-semi-pinacol variants.[14,15] As such, the oxidative conditions required to promote SET and subsequent rearrangement, as opposed to the acid-catalyzed conditions

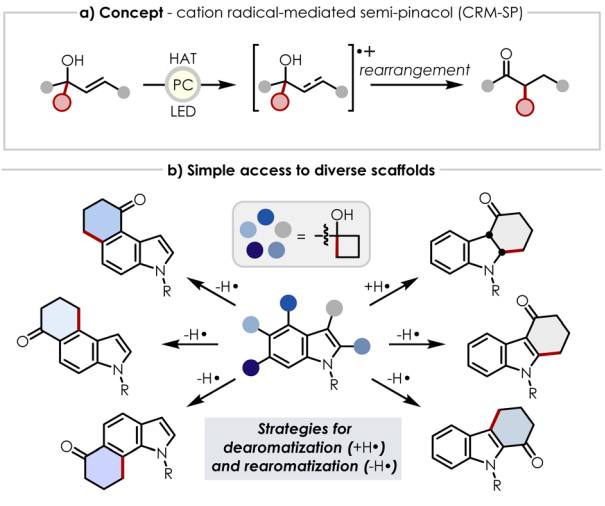

Scheme 1 (a) Concept for a cation radical-mediated semi-pinacol type rearrangement (CRM-SP). (b) Diversification of the indole scaffold using ring expansion methodology. [a]Strategies for both dearomatization and rearomatization are indicated by the addition or removal of a hydrogen atom, respectively.

Department of Chemistry, University of North Carolina at Chapel Hill, Chapel Hill, North Carolina 27599-3290, USA. E-mail: nicewicz@email.unc.edu

† B. B. F. and C. T. O. contributed equally to this work.

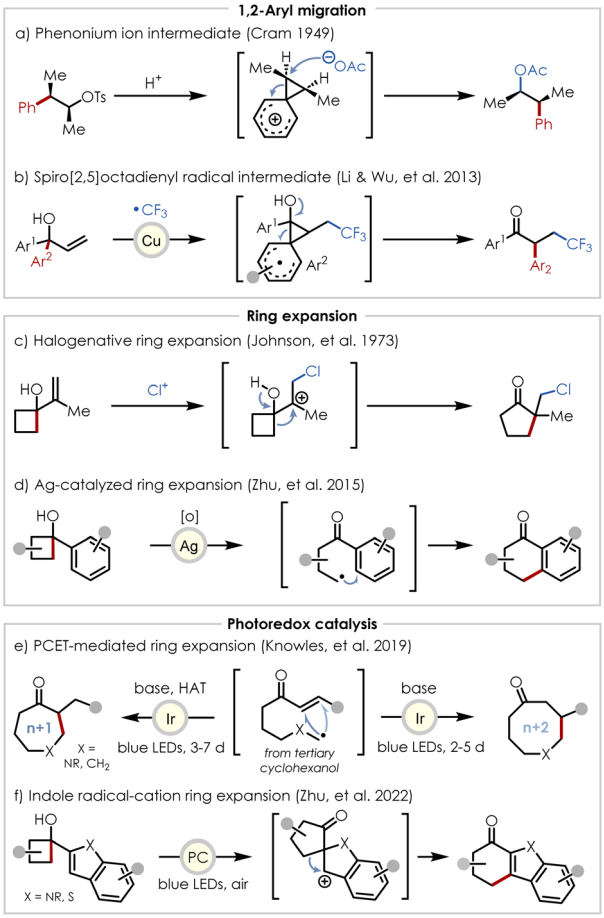

Scheme 2 Overview of literature precedent for related ring expansion methodologies, highlighting reactions of historical importance and key steps of their proposed mechanisms.

typically seen in semi-pinacol-like rearrangements, potentially offer differential functional group tolerance and provide an alternative logic for synthetic strategy.

Additionally, we envisioned that a photocatalyst with an appropriately high excited state reduction potential could be used to extend this chemistry beyond simple alkenyl or styrenyl compounds to enable oxidation of more challenging substrates such as benzenoids and heterocycles.[16] An example of this concept as it might be applied to the indole backbone is also shown in Scheme 1b, illustrating the potential to access a wide range of polycyclic scaffolds *via* the ring expansion of a cyclobutanol appended to various positions on both the pyrrole and the benzene portions of the parent indole.

Our preliminary mechanistic hypothesis for the case of a 1,2-shift involved direct interaction of the migrating group with the cation radical, which – in the case of an aryl migrating group adjacent to a styrenyl acceptor – would lead to a spiro[2,5] octadienyl cation radical transition state with the spin density of the radical located at the benzylic position of the styrenyl fragment (see mechanistic discussion below). While intermediate phenonium ions generated by nucleophilic interaction of aryl groups with neighboring electrophilic centers have been well-documented (Scheme 2a),[17–21] and cases in which a radical engages the aryl group have been invoked in reports such as the trifluoromethylation-induced radical 1,2-aryl migration reported by Li and Wu (Scheme 2b),[22–24] to the best of our knowledge no examples of the proposed cation radical transition state have been previously documented.

Examples of cyclobutanol ring expansions date back to the 1970's with reports such as Johnson's chlorinative semi-pinacol *n*+1 ring expansion yielding 5-*exo-trig* products (Scheme 2c).[25] More recently, ring fusion of cyclobutanols with various aromatic groups has been demonstrated by Zhu in which silver(II)-mediated alkoxy radical generation was proposed to induce β-scission and subsequent intramolecular capture of the resulting alkyl radical by the aromatic group at the position *ortho* to the newly generated acyl group (Scheme 2d).[26] Photoredox catalyzed ring expansions of cyclic tertiary alcohols have also appeared in recent literature with a notable example being Knowles' expansions of 5- and 6-membered rings to *n*+1 (*exo-trig*) and *n*+2 (*endo-trig*) adducts – differentially achieved by the incorporation or omission of a hydrogen atom transfer (HAT) reagent – which is proposed to proceed by alkoxy radical generation *via* a proton-coupled electron transfer (PCET) mechanism (Scheme 2e).[27–31] In addition, indoles and benzothiophenes have been successfully employed in ring fusions with substituted cyclobutanols in Zhu's total synthesis of Uleine, though only the C2-substituted heterocycles were studied (Scheme 2f).[32] However, rather than invoking alkoxy radical generation, their mechanistic experiments suggest that upon oxidation of the heterocycle, a semi-pinacol rearrangement generates a C2-spirocyclic radical intermediate, which upon further oxidation to produce a benzylic cation radical, undergoes a Wagner-Meerwein 1,2-alkyl shift followed by rearomatization to yield tetrahydrocarbazol-1-ones and their thio-counterparts.

In this report we probe the feasibility, through experiment and calculation, of spiro[2,5]octadienyl cation radical transition states in 1,2-aryl shifts and explore the extensions of this transformation to other migratory and acceptor functional groups. These studies led us to the development of two mechanistically distinct transformations – a cation radical-mediated semi-pinacol (CRM-SP) reaction and an *n*+2 ring expansion of cyclobutanols – along with strategies for trapping non-aromatic

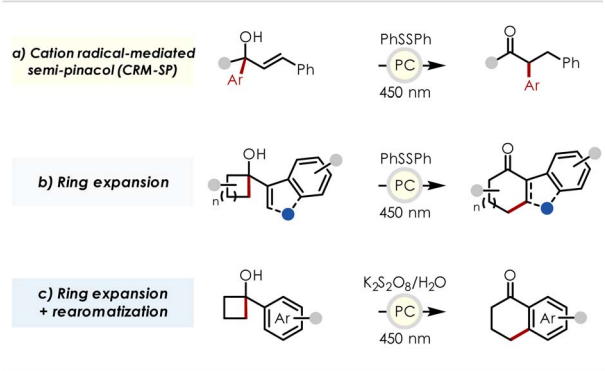

Scheme 3 Overview of photoredox mediated transformations presented herein.

intermediates or isolating the rearomatized products through the use of hydrogen atom donating or accepting reagents, respectively (Scheme 3).

Results and discussion

Our preliminary investigations began with a chalcone-derived tertiary alcohol, which proved capable of undergoing photooxidation-induced rearrangement to ketone product in a 12% yield in dichloroethane at a concentration of 150 mM (Table 1, entry 1). After a series of control experiments (entries 2–5), we identified acetonitrile as the most suitable solvent (entries 6–8) which provided the rearranged product in 50% yield after decreasing the concentration to 10 mM (entry 9). Attempts to reduce the reaction time (entries 10–11) and the addition of base (2,6-lutidine, entry 12) led to decreased yields while the use of other turnover reagents (thiophenol, entry 13) or alternative acridinium photocatalysts with lower or higher excited state reduction potentials (entries 14–15) inhibited the reactivity almost entirely.

We then turned our attention toward ring expansion variants, which could facilitate skeletal rearrangements of complex molecular scaffolds with sensitive functionality. Still under the presupposition that the semi-pinacol-like mechanism discussed above was operative, we were somewhat surprised when a cyclobutanol substrate resulted in the formation of 6-*endo-trig* ring-expanded 2-phenylcyclohexan-1-one product in 45% yield

Table 1 Condensed optimization table for cation radical-mediated semi-pinacol (CRM-SP)[a]

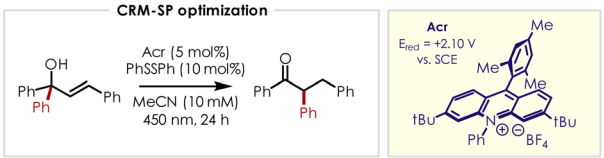

Entry	Deviation from standard conditions	Yield (%)
1	Initial hit: DCE (150 mM)	12
2	DCE (150 mM), no Acr	N.D.
3	DCE (150 mM), no PhSSPh	N.D.
4	DCE (150 mM), no LED	N.D.
5	DCE (150 mM), 5 °C	<5
6	MeOH (75 nM)	N.D.
7	TFE (75 mM)	26
8	MeCN (75 mM)	39
9	None	50
10	3 h	15
11	6 h	25
12	2,6-Lutidine	34
13	PhSH, no PhSSPh	N.D.
14	PC: **Acr 2** (+1.65 V)	N.D.
15	PC: **Acr 3** (+2.21 V)	<5

[a] Yields determined by ^{1}H NMR spectroscopy. The full optimization table along with the structures for **Acr 2** and **Acr 3** are presented in Table S4.

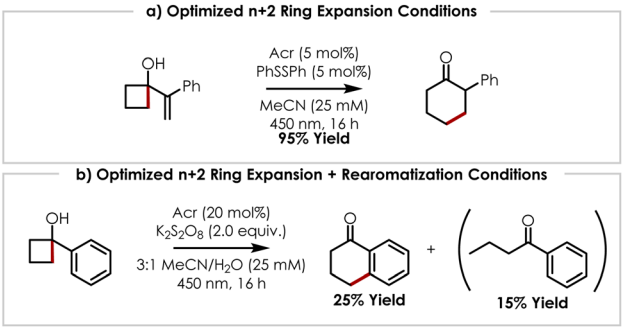

Scheme 4 Optimized conditions for (a) *n*+2 ring expansion and (b) *n*+2 ring expansion + rearomatization. [a]Yields determined by ^{1}H NMR spectroscopy. Full optimization tables are available in the SI (Tables S5 and S8).

under our previously optimized conditions, rather than the 5-*exo-trig* cyclopentanone that would be expected from a concerted 1,2-alkyl shift. Further optimization yielded 95% of the ring expanded product when run in anhydrous acetonitrile (Scheme 4a). As none of the 5-*exo-trig* product was detectable in the crude reaction mixture *via* ^{1}H NMR, we began to speculate that this ring expansion might be mechanistically distinct from the 1,2-aryl shift. This result is also notably in contrast to what would be predicted using general radical ring closure guidelines and arguments of kinetic favorability.[33,34]

The hypothesis that diverging mechanistic pathways might be operative was further supported by the isolation of tetralone without the presence of any dearomatized spirocyclic product. Initial attempts to utilize the same conditions as those used for the *n*+2 ring expansion discussed above proved unsuccessful, but fortunately the addition of potassium persulfate, as used in the silver-catalyzed methodology reported by Zhu, *et al.*,[26] led to formation of the desired tetralone, albeit in low yield. While in the Zhu report, the persulfate anion was used to oxidize silver(I) to silver(II), we speculated that it might serve an alternative role in our chemistry by removal of a hydrogen atom at the end of the catalytic cycle to restore aromaticity *via* either the sulfate ion or its radical anion counterpart generated after turnover of the acridinium catalyst. Notably, these conditions also resulted in the formation of cleavage product, 1-phenylbutan-1-one, lending further evidence to a stepwise rather than concerted mechanism. Further optimization ultimately provided a modest 25% yield of tetralone and 15% cleaved product when catalyst loading was increased to 20 mol% (Scheme 4b).

With satisfactory conditions in hand for the ring expansion, we were pleased to find that a gram-scale (5.74 mmol) reaction was possible in a 250 mL oval-shaped recovery flask with vigorous stirring and increased concentration (50 mM; to reduce the size of the reaction vessel), enabling the synthesis of 2-phenylcyclohexan-1-one in 62% yield (Scheme 5a). The reaction also proved viable at the gram scale under continuous flow conditions, affording a 48% yield using a recirculation approach and a flow cell with a residence time of approximately 6.5 minutes, which over the course of 16 h resulted in a total solution exposure time of approximately 1 hour (Scheme 5b).[35]

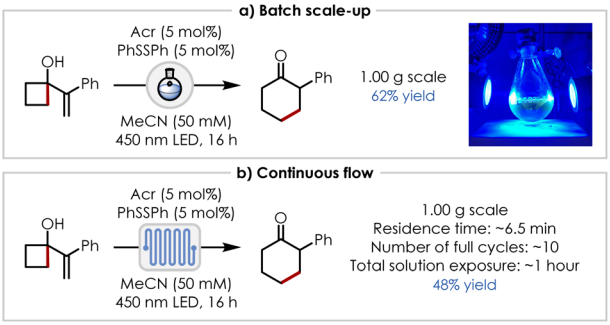

Scheme 5 Scale-up of *n*+2 ring expansion: (a) batch scale up, (b) continuous flow. [a]Details of setup, additional parameters, and equations for their calculation are given in the SI.

After performing these optimizations, we sought to probe the limitations of each reaction class. An overview of successful substrates is shown in Scheme 6. From these results it can be seen that the CRM-SP is somewhat narrow in its applicability (an overview of unsuccessful substrates are provided in the SI), with the migratory acceptor being limited to styrenes (**1–3**). However, the identity of the migrating group is more flexible as demonstrated by the migration of an *N*-tosyl protected indole in the synthesis of **3**. The ring expansion chemistry, in contrast, is quite robust and shows a high tolerance for various functional groups including protected secondary amines (**9–10**), ethers (**11–12**), esters (**13**), carbamates (**24**), sulfonamides (**9**, **22–23**, **25–26**), and various heterocycles (**15**, **21–27**). Both the styrenyl unit and the carbocyclic portion of the cyclic tertiary alcohol can also be altered substantially, with tolerance of constrained styrenes (indoles (**21–24**), oxazoles (**27**), indenes (**17**), and various carbocycles (**18–20**)) and a range of substitution on the cyclobutane moiety – including spirocyclic (**8–10**) and bicyclic (**16**, **20**) ring junctions. In addition to cyclobutanols, the three-membered cyclopropanol counterpart (**32**) also proved successful along with styrenes featuring the cyclobutanol at the β-position (**31**), rather than the α-position. The reaction proved especially robust for modification of the indole scaffold with examples **21** through **26** demonstrating substitution at C2 through C6 of the indole nucleus. Of particular note, both indoline **22** and indole **23** could be obtained in moderate yield

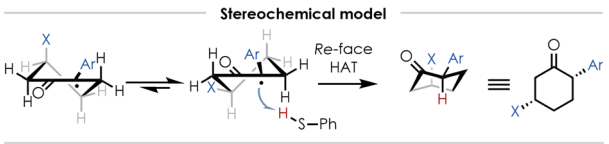

Fig. 1 Stereochemical model showing the most stable chair conformer and the facial selectivity of HAT by the substrate.

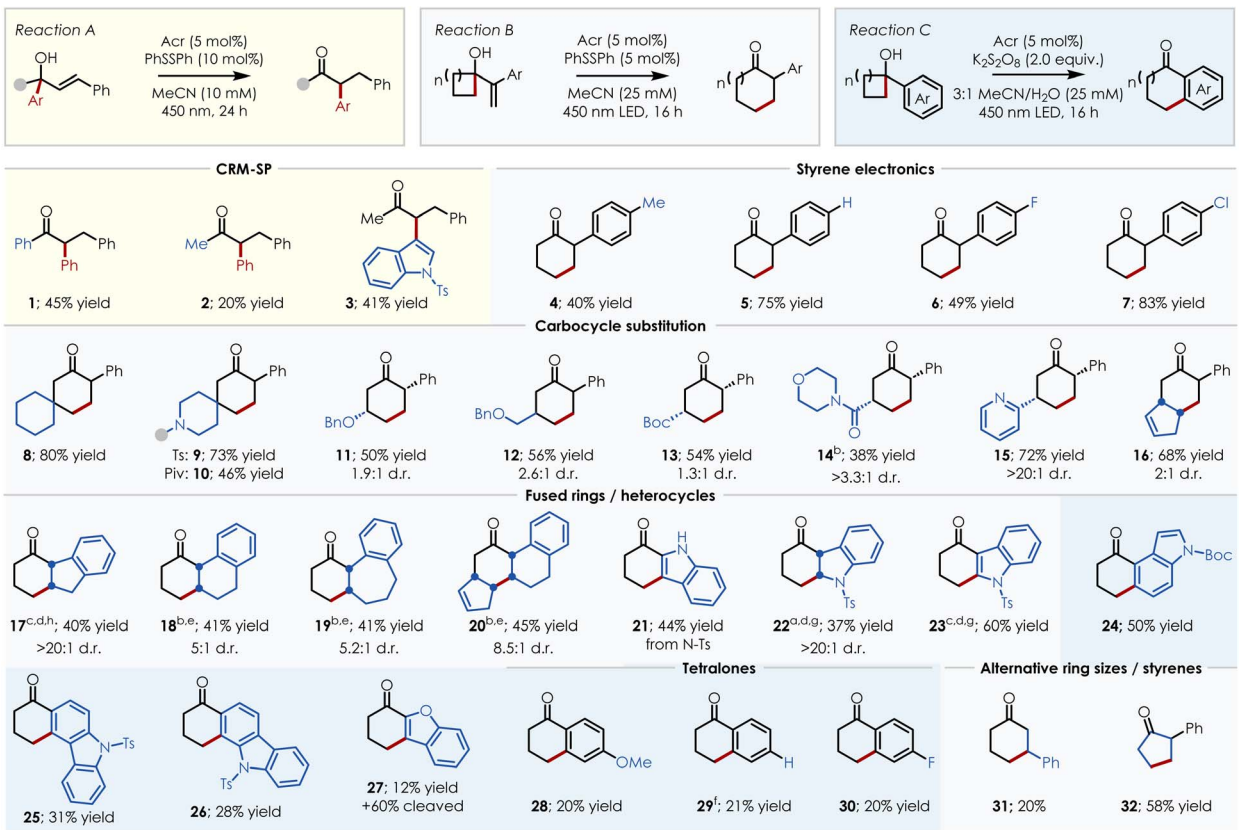

Scheme 6 Substrate scope for rearrangement reaction. *(Reaction A – yellow boxes) Substrate scope for CRM-SP. (Reaction B – grey boxes) Substrate scope for *n*+2 ring expansion. (Reaction C – blue boxes) Substrate scope for *n*+2 ring expansion with subsequent rearomatization. Yields refer to isolated yields. Deviations from standard conditions – time: [a]24 h, [b]40 h, [c]48 h; catalyst loading: [d]10 mol%, [e]15 mol%, [f]20 mol%; diphenyl disulfide loading: [g]10 mol%; alternative catalyst: [h]Xan. See SI for further details.

using this chemistry with the reaction time being the only parameter changed (16 h *vs.* 48 h, respectively). Additionally, 1,2-dihydronaphthalene-derived bicyclic compound **20** enables the synthesis of the carbon skeleton found in steroids.

We hypothesize that the stereochemical determining step is HAT, the facial selectivity of which is governed by kinetics. Fig. 1 depicts this stereochemical model, highlighting the preference of the cyclohexanone to adopt a conformation allowing the X substituent to occupy a pseudo-equatorial orientation which facilitates hydrogen atom abstraction by the less-sterically hindered *Re* face leading to predominantly the *cis* configuration *via* a Fürst–Plattner-type transition state.[36]

To gain insight about our speculative mechanistic pathways, we first turned toward computational methods to probe the feasibility of various routes along the energetic landscape.[37–43] Fig. 2 shows a comparison between the concerted pathway (red arrows) *vs.* a PCET pathway in which an aryl radical is expelled and subsequently re-engages with the formed α,β-unsaturated ketone (black and grey arrows). In the case of the concerted pathway, the energetic barrier that must be surpassed to reach the spiro[2,5]octadienyl cation radical transition state is approximately 8.0 kcal mol^{-1} and is calculated to be exothermic (−7.3 kcal mol^{-1}). In contrast, the barrier for the PCET route requires surpassing an energy barrier of 15.7- kcal mol^{-1} to expel an aryl radical which additionally leads to a less thermodynamically stable product (+0.7 kcal mol^{-1} relative to the alkoxy radical). While this calculation is somewhat simplified – the protonation states and order of events have been assumed – it does lend credence to the hypothesis that a semi-pinacol-like mechanism might be involved, as the expulsion of an aryl radical is both kinetically and thermodynamically unfavorable. This corroborates the experimental lack of observance of the 1,4-addition product.

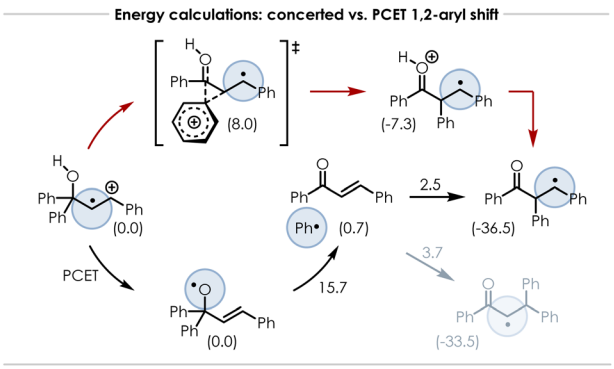

Fig. 2 Energy calculations for possible mechanistic pathways of the 1,2-aryl shift. (Red arrows) Concerted 1,2-aryl shift with $\Delta G^{\ddagger} = 8.0$ kcal mol; kinetically favorable pathway. (Black arrows) PCET and subsequent aryl radical expulsion with $\Delta G^{\ddagger} = 15.7$ kcal mol^{-1}, followed by 1,3-addition. (Grey arrow) Energy barrier and product stability for 1,4-addition to the α,β-unsaturated ketone by the aryl radical. Both the concerted and PCET pathway starting materials have been set to 0.0 kcal mol^{-1} for comparison. Calculated at the wB97XD/Def2TZVP level of theory with implicit modeling of MeCN (See SI for details).

While the concerted rearrangement process appeared energetically feasible for the 1,2-aryl shift, we were hesitant to invoke this mechanism for the ring expansion as the resulting bicyclic transition state would require a high degree of organization and be both highly strained and less accommodating to stabilization of positive charge. As such, we reasoned that the ring expansion might be more likely to undergo a stepwise mechanistic pathway in which upon generation of an analogous alkoxy radical by PCET, β-scission occurs followed by 6-*endo-trig* Giese addition to the α,β-unsaturated ketone by the resulting primary radical. By comparing the 5-*exo-trig* and 6-*endo-trig* stepwise transition states, it becomes clear that the 5-*exo-trig* transition state suffers from a 1,3-diaxial interaction between the methyl group and an axial hydrogen atom when in the envelope conformation, whereas the 6-*endo-trig* cyclization allows the phenyl substituent to adopt a pseudo-axial conformation and thus experiences less sterically-induced strain.

Examination of the related energy landscape provides further support for the 6-*endo-trig* pathway as shown in Fig. 3 (left). Ring opening of the cyclobutane moiety is calculated to only require the summit of a 1.0 kcal mol^{-1} hurdle and leads to primary radical formation approximately 21.9 kcal mol^{-1} lower in energy – as expected considering the relief of ring strain. We additionally examined the possibility of neighboring group

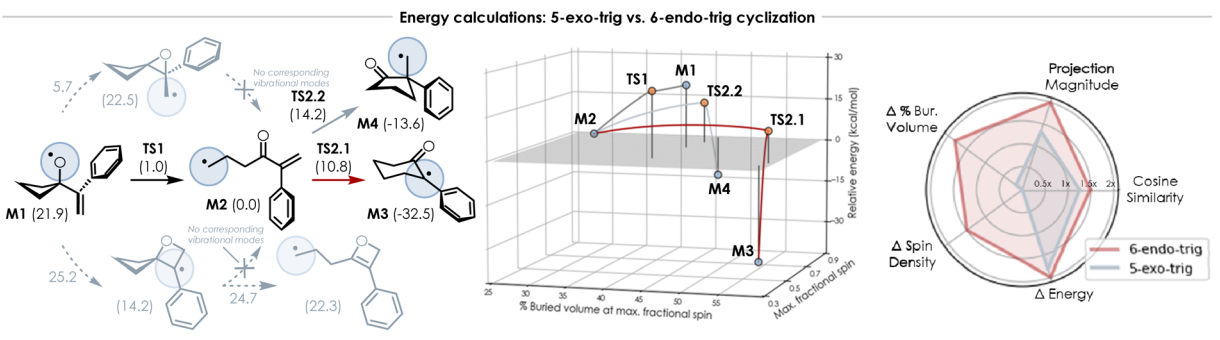

Fig. 3 Energy calculations for possible mechanistic pathways of the *n*+2 ring expansion. (Black arrow) Cyclobutanol ring opening. (Red arrow) 6-*endo-trig* cyclization. (Grey arrow) 5-*exo-trig* cyclization. (Dotted grey arrows) Epoxide and oxetane pathways. (Middle) 3D plot of relative energy (*z* – axis; kcal mol^{-1}), maximum fractional spin density (*y*-axis) and percent buried volume (*x*-axis) at the associated radical center. (Right) Comparison of the 5-*exo-trig* and 6-*endo-trig* pathways *vs.* a dataset of known radical reaction pathways *via* trajectory analysis. Calculated at the wB97XD/Def2TZVP level of theory with implicit modeling of MeCN (See SI for calculation details).

assistance for cleavage through either epoxide or oxetane intermediates, but both were found to have significantly higher barriers and lacked productive vibrational modes that could lead to ring opened or expanded products. These calculations also provided more concrete support for the 6-*endo-trig* pathway over 5-*exo-trig* with a $\Delta\Delta G^{\ddagger}$ of approximately 3.4 kcal mol^{-1}. Also shown in Fig. 3 (middle) is a three-dimensional plot of energy (*z*-axis) *vs.* a pair of radical stability metrics – maximum fractional spin density (*y*-axis) and percent buried volume (*x*-axis) at the associated radical center – proposed by St. John and Paton.[44] As is further discussed in the SI, a favorable radical reaction tends to follow a trajectory that proceeds downhill in energy (decrease on *z*-axis), distributes its spin density over a wider portion of the molecule (decrease on *y*-axis), and positions the radical in a region of the molecule that is more sterically shielded (increase on *x*-axis). From this plot, it can be seen that the 6-*endo-trig* path (red lines) follows this ideal trend more closely, as compared to the 5-*exo-trig* path (grey lines). This method of plotting also lends insight into structural features of the reaction intermediates and transition states that would be lacking in a standard diagram of energy alone, as one can assess the similarity of these species and obtain a sense of "earliness" or "lateness" as described by Hammond's postulate.[45] For both ring closing pathways in this instance, visual inspection indicates late transition states, and thus closer similarity to the cyclized species, as these points lie closer to products than starting materials. To provide support for this idea of an "ideal trajectory", we performed this analysis on a set of nine known radical reactions to determine the average change in each of these three quantities over the course of their respective reaction trajectories. From this analysis we obtained values of −19.47 kcal mol^{-1} for the average Δ energy, +7.88 units for the average Δ percent buried volume, and −0.20 units for the average Δ maximum fractional spin density, confirming the sense of direction one would expect based on arguments of energy and radical stability. To compare the favorability of our ring closing pathways both between each other and against the dataset, we performed a trajectory analysis (see SI for details) and used a radial plot in which 6-*endo-trig* is represented by red, 5-*exo-trig* is represented by grey, and the dataset is depicted as circles radiating from the origin where 1x represents the average values and 2x represents doubling of the average values. From this plot it can be seen that 6-*endo-trig* is more favorable than 5-*exo-trig* according to all associated metrics.

As we suspected that the 1,2-aryl shift and the *n*+2 ring expansion were likely proceeding through different mechanisms, we wondered if structural features of the cation radical common to the first step of each reaction might aid in rationalizing this divergence. Fig. 4 shows the symbolic representation, an overlay of calculated low energy conformations, and the lowest unoccupied molecular orbital for each species. Interestingly, the preferred conformation is different for each, with the styrene fragment of the chalcone-derived substrate positioned parallel to the alcohol, while for the cyclobutanone-derived substrate this fragment is positioned perpendicular. This in turn results in different orientations of the LUMO with respect to the alcohol – a feature that could affect the ability of the

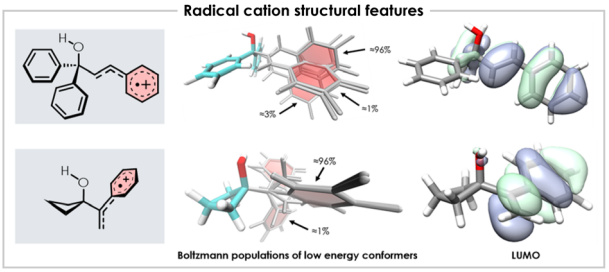

Fig. 4 Comparison of structural features of the cation radical for the chalcone- and cyclobutanone-derived species. (Middle) Overlay of low energy styrene conformations with arrows specifying weighted contributions. (Right) LUMO isosurface highlighting the orientation of the orbitals for the lowest energy conformation relative to the alcohol. Ensembles obtained using xTB/CREST at the GFN2-xTB level of theory and optimized at the wB97XD/Def2TZVP level of theory with implicit modeling of MeCN (See SI for details).

styrenyl cation radical to accept an electron from the alcohol under a PCET pathway.

The hypothesis that acceptor orientation relative to the alcohol might affect divergence of mechanism is also reinforced by both our successful and unsuccessful substrate scope (see SI). While the chalcone-derived species prefers a parallel arrangement, the analogous case with substitution at the α-position of the styrene (1,1,2-triphenylprop-2-en-1-ol) exhibits a much larger steric clash between the styrenyl unit and the adjacent alcohol – leading to a perpendicular orientation between the two. Following the proposed logic, we expect this analogous substrate to be capable of proceeding through the PCET pathway. Accordingly, we observed the formation of benzophenone which is proposed to be accessed by alkoxy radical formation *via* PCET and subsequent β-scission. Additional supporting evidence can be inferred from the reduced yield of compound **31** relative to **5**, which could be due to its large increase in flexibility and potential decrease in PCET efficiency.

We then performed a series of experiments to probe various aspects of our mechanistic hypotheses – summarized in Scheme 7 along with relevant reaction rates. We first verified the formation of positive charge by the addition of pyrazole as a nucleophilic trapping agent (Scheme 7a). From this experiment we observed isolable quantities (20%) of anti-Markovnikov pyrazole-trapped cyclobutanol **33** along with 55% of ring expanded product **5** – regiochemistry consistent with our lab's prior experience with styrenyl cation radical functionalization.[46–49] As evidence for β-scission (Scheme 7b), we had observed cleaved products – easily identifiable by the distinct peaks of the propyl chain in ^{1}H NMR – during our optimization studies of compounds containing aryl groups (*i.e.* phenyl) and heterocycles (indoles, benzofurans). Of note however, only trace amounts (<5%) of the cleaved product was detected for the prototypical styrene substrates. Additional support for the β-scission pathway was uncovered during our attempts to induce rearrangement of a tetramethyl-substituted cyclobutanol. In this case, we detected not only formation of

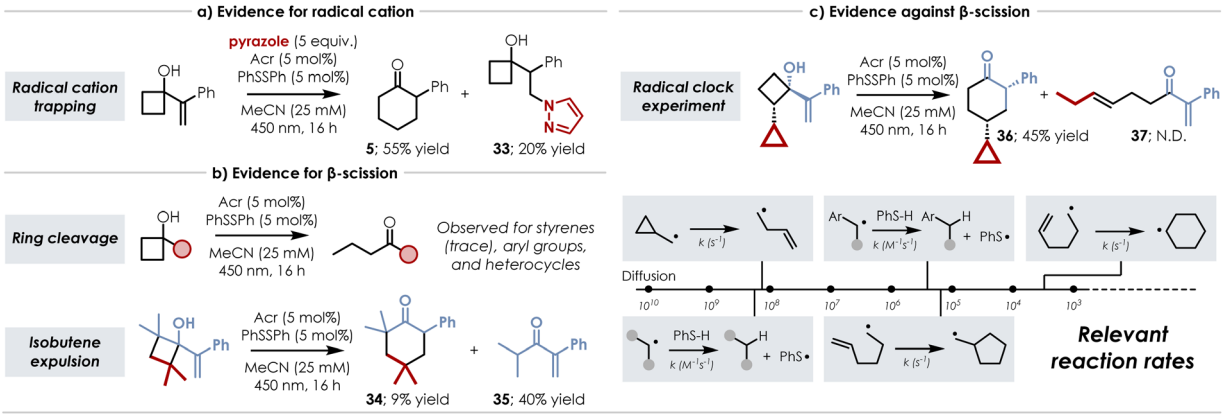

Scheme 7 Experimental mechanistic probes and relevant radical reaction rates. (a) Cation radical trapping experiment using 5.0 equiv. pyrazole. (b) Experiments supporting a β-scission pathway. (Top) Observation of ring-opened products for styrenes (trace), aryl groups, and heterocycles. (Bottom) Attempts at ring-expanding a tetrame-thyl derivative lead to expulsion of isobutene. (c) Cyclopropane radical clock experiment exhibiting no cyclopropane cleavage and thus providing conflicting evidence against β-scission. (Bottom right) Relevant reaction rates for various radical processes. All yields shown are percent yields obtained by ^{1}H NMR spectroscopy using HMDSO as an internal standard.

the apparent *n*+2 ring expanded product **34** (9% yield), but also the formation of α,β-unsaturated ketone **35** (40% yield) which is formed after expulsion of isobutene – presumably after cyclobutane cleavage. However, an additional experiment in which a cyclopropane was appended at the position α-to the alcohol yielded conflicting evidence as this radical clock remained intact over the course of the reaction with ring expanded product **36** being isolated in 12% yield and no detectable quantities of cyclopropane-opened alkene **37** (Scheme 7c). While it could be argued that the Giese addition occurs faster than ring opening of the cyclopropane, this seems unlikely as the rates of the prototypical systems differ by approximately 10^5 s^{-1}. Although these results are somewhat inconclusive, they suggest that there could be a divergence in mechanism that is substrate dependent. Alternatively, it could be conceived that as the carbon–carbon bond of the cyclobutane begins to cleave, favorable interactions between the primary radical and the styrenyl π* orbital occur before the propyl chain can fully extend – an interaction possibly promoted by maintenance of their close proximity by the surrounding solvent cage.

An overview of these potential mechanisms is summarized by Scheme 8. Scheme 8a shows the proposed mechanism for the CRM-SP in which the acridinium photocatalyst is first excited by 450 nm light to reach the excited state which removes an electron from the styrenyl fragment of the tertiary alcohol to yield a cation radical. This positive charge then induces a concerted semi-pinacol-like 1,2-migration of the phenyl group, resulting in the formation of a carbon-oxygen double bond and a benzylic radical. Completion of the catalytic cycle is then incurred after turnover of the reduced acridinium catalyst *via* SET to the thiophenolate radical (generated by exposure of diphenyl disulfide to 450 nm light) which subsequently abstracts a proton and donates a hydrogen atom to the benzylic radical – yielding the ketone product. Caveats not included in this working mechanism include precise state of protonation for the intermediates and the possibility that the semi-pinacol-like shift is promoted by basic species in the reaction medium.

Scheme 8b shows a plausible mechanism for the *n*+2 ring expansion with the catalytic cycle analogous to that of the CRM-SP. The differentiating step for this mechanism comes after generation of the cation radical which can potentially act as an

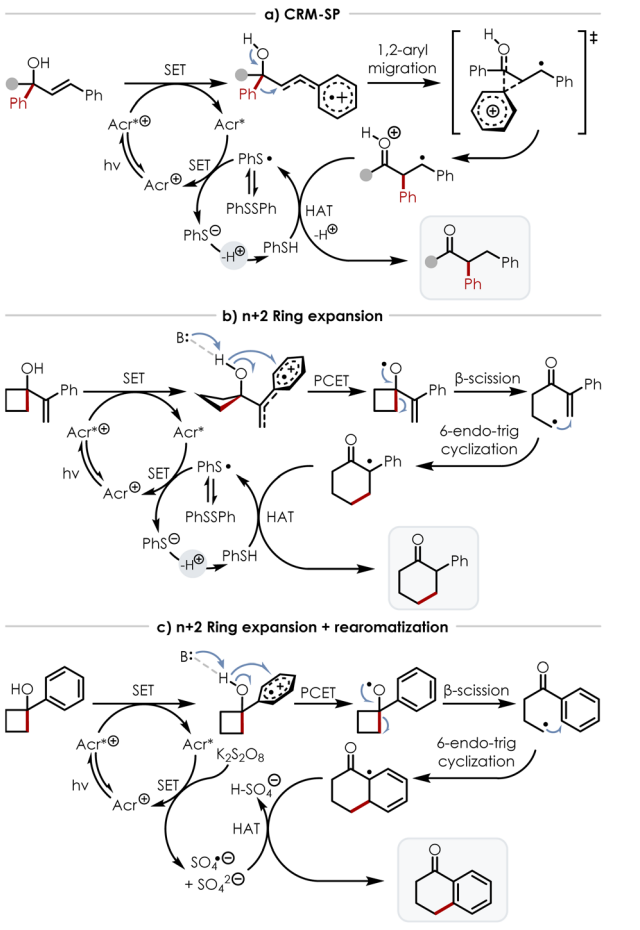

Scheme 8 Plausible mechanisms: (a) CRM-SP (b) *n*+2 ring expansion (c) *n*+2 ring expansion with rearomatization.

electron hole to facilitate PCET from the adjacent alcohol with assistance from a general basic species – possibly the thiophenolate anion. This results in an alkoxy radical that can then undergo β-scission to relieve strain from the cyclobutane ring and reveal a reactive primary radical. This primary radical can then add to the resulting α,β-unsaturated ketone in a Giese addition, yielding a benzylic radical, which after abstracting a hydrogen atom from thiophenol, yields the ring expanded ketone product. For the case of the *n*+2 ring expansion with rearomatization, the mechanism differs only by the means of catalyst turnover (*via* potassium persulfate rather than diphenyl disulfide) and the terminal step in which a hydrogen atom is removed from, rather than donated to, the final intermediate (Scheme 8c).

Conclusions

To expand the toolbox of transformations enabled by organic photoredox catalysis, we have developed a set of three rearrangement reactions – a cation radical-mediated semi-pinacol reaction, an *n*+2 ring expansion, and an *n*+2 ring expansion with rearomatization – which are widely applicable to the synthesis of natural product scaffolds and enable access to unique areas of chemical space that could prove useful for medicinal chemistry. We also demonstrated the scalability of the ring expansion under both batch and continuous flow conditions at the gram scale.

In addition to showcasing a diverse substrate scope, we performed a series of computational and experimental studies to probe feasible mechanisms. These studies led us to propose potentially substrate-dependent mechanisms which proceed through either concerted semi-pinacol-like rearrangement or *via* a sequence of PCET, β-scission, Giese addition, and terminal HAT.

Author contributions

B. B. F. and C. T. O. contributed equally to this work.

Conflicts of interest

There authors declare no conflict of interest.

Data availability

Supplementary information (SI): experimental procedures; optimization and controls; materials and methods; high-resolution mass spectrometry (HRMS) data; ^{1}H and ^{13}C NMR spectra; computational methods and data. See DOI: https://doi.org/10.1039/d5sc08977h.

Abbreviations

PC	Photocatalyst
SET	Single electron transfer
HAT	Hydrogen atom transfer
PCET	Proton-coupled electron transfer
CRM-SP	Cation radical-mediated semi-pinacol
NMR	Nuclear magnetic resonance
HMDSO	Hexamethyldisiloxane
DCE	Dichloroethane
TFE	Trifluoroethanol
TFT	Trifluorotoluene
LUMO	Lowest unoccupied molecular orbital
xTB	Extended tight-binding
CREST	Conformer rotamer ensemble sampling tool

Acknowledgements

Financial support was provided in part by the National Institute of Health (NIGMS) Award R35 GM136330. The authors would like to thank the University of North Carolina's Department of Chemistry NMR Core and Mass Spectrometry Core Laboratories for the use of their instrumentation. Additionally, the authors would like to acknowledge Dr Jeremy D. Griffin for their preliminary work on the aryl migration chemistry.

References

1 L. Chen, G. Li and L. Zu, *Org. Chem. Front.*, 2022, **9**, 5383–5394.
2 X. Wu, Z. Ma, T. Feng and C. Zhu, *Chem. Soc. Rev.*, 2021, **50**, 11577–11613.
3 N. A. Romero and D. A. Nicewicz, *Chem. Rev.*, 2016, **116**, 10075–10166.
4 M. Schmittel and A. Burghart, *Angew Chem. Int. Ed. Engl.*, 1997, **36**, 2550–2589.
5 A. Padwa, C. S. Chou and W. F. Rieker, *J. Org. Chem.*, 1980, **45**, 4555–4564.
6 H. D. Roth, M. L. M. Schilling, P. G. Gassman and J. L. Smith, *J. Am. Chem. Soc.*, 1984, **106**, 2711–2712.
7 C. J. Abelt, H. D. Roth and M. L. M. Schilling, *J. Am. Chem. Soc.*, 1985, **107**, 4148–4152.
8 K. Lorenz and N. L. Bauld, *J. Catal.*, 1985, **95**, 613–616.
9 T. Miyashi, A. Konno and Y. Takahashi, *J. Am. Chem. Soc.*, 1988, **110**, 3676–3677.
10 L. Lopez and L. Troisi, *Tetrahedron Lett.*, 1989, **30**, 3097–3100.
11 L. Lopez, G. Mele, V. Fiandanese, C. Cardellicchio and A. Nacci, *Tetrahedron*, 1994, **50**, 9097–9106.
12 D. W. Reynolds, B. Harirchian, H.-S. Chiou, B. K. Marsh and N. L. Bauld, *J. Phys. Org. Chem.*, 1989, **2**, 57–88.
13 N. L. Bauld, *J. Comput. Chem.*, 1990, **11**, 896–898.
14 Z.-L. Song, C.-A. Fan and Y.-Q. Tu, *Chem. Rev.*, 2011, **111**, 7523–7556.
15 M. A. S. Blackburn, C. C. Wagen, M. R. Bodrogean, P. M. Tadross, A. J. Bendelsmith, D. A. Kutateladze and E. N. Jacobsen, *J. Am. Chem. Soc.*, 2023, **145**, 15036–15042.
16 A. R. White, L. Wang and D. A. Nicewicz, *Synlett*, 2019, **30**, 827–832.
17 D. J. Cram, *J. Am. Chem. Soc.*, 1949, **71**, 3863–3870.

18 D. J. Cram, *J. Am. Chem. Soc.*, 1964, **86**, 3767–3772.
19 H. C. Brown, K. J. Morgan and F. J. Chloupek, *J. Am. Chem. Soc.*, 1965, **87**, 2137–2153.
20 G. A. Olah, M. B. Comisarow, E. Namanworth and B. G. Ramsey, *J. Am. Chem. Soc.*, 1967, **89**, 5259–5265.
21 S. Nagumo, M. Ono, Y. Kakimoto, T. Furukawa, T. Hisano, M. Mizukami, N. Kawahara and H. Akita, *J. Org. Chem.*, 2002, **67**, 6618–6622.
22 X. Liu, F. Xiong, X. Huang, L. Xu, P. Li and X. Wu, *Angew. Chem., Int. Ed.*, 2013, **52**, 6962–6966.
23 H. Lindner and E. M. Carreira, *Angew. Chem., Int. Ed.*, 2024, **63**, e202407827.
24 D. Lunic, N. Vystavkin, J. Qin and C. J. Teskey, *Angew. Chem.*, 2024, **136**, e202409388.
25 C. R. Johnson and R. W. Herr, *J. Org. Chem.*, 1973, **38**, 3153–3159.
26 J. Yu, H. Zhao, S. Liang, X. Bao and C. Zhu, *Org. Biomol. Chem.*, 2015, **13**, 7924–7927.
27 K. Zhao, K. Yamashita, J. E. Carpenter, T. C. Sherwood, W. R. Ewing, P. T. W. Cheng and R. R. Knowles, *J. Am. Chem. Soc.*, 2019, **141**, 8752–8757.
28 H. G. Yayla, H. Wang, K. T. Tarantino, H. S. Orbe and R. R. Knowles, *J. Am. Chem. Soc.*, 2016, **138**, 10794–10797.
29 E. Tsui, H. Wang and R. R. Knowles, *Chem. Sci.*, 2020, **11**, 11124–11141.
30 E. C. Gentry and R. R. Knowles, *Acc. Chem. Res.*, 2016, **49**, 1546–1556.
31 L. Huang, T. Ji and M. Rueping, *J. Am. Chem. Soc.*, 2020, **142**, 3532–3539.
32 A. Leclair, Q. Wang and J. Zhu, *ACS Catal.*, 2022, **12**, 1209–1215.
33 A. L. J. Beckwith, C. J. Easton and A. K. Serelis, *J. Chem. Soc. Chem. Commun.*, 1980, 482–483.
34 K. Gilmore, R. K. Mohamed and I. V. Alabugin, *Wiley Interdiscip. Rev.: Comput. Mol. Sci.*, 2016, **6**, 487–514.
35 M. B. Plutschack, B. Pieber, K. Gilmore and P. H. Seeberger, *Chem. Rev.*, 2017, **117**, 11796–11893.
36 A. Fürst and Pl. A. Plattner, *Helv. Chim. Acta*, 1949, **32**, 275–283.
37 M. J. Frisch, G. W. Trucks, H. B. Schlegel, G. E. Scuseria, M. A. Robb, J. R. Cheeseman, G. Scalmani, V. Barone, G. A. Petersson, H. Nakatsuji, X. Li, M. Caricato, A. V. Marenich, J. Bloino, B. G. Janesko, R. Gomperts, B. Mennucci, H. P. Hratchian, J. V. Ortiz, A. F. Izmaylov, J. L. Sonnenberg, D. Williams-Young, F. Ding, F. Lipparini, F. Egidi, J. Goings, B. Peng, A. Petrone, T. Henderson, D. Ranasinghe, V. G. Zakrzewski, J. Gao, N. Rega, G. Zheng, W. Liang, M. Hada, M. Ehara, K. Toyota, R. Fukuda, J. Hasegawa, M. Ishida, T. Nakajima, Y. Honda, O. Kitao, H. Nakai, T. Vreven, K. Throssell, J. A. Montgomery Jr, J. E. Peralta, F. Ogliaro, M. J. Bearpark, J. J. Heyd, E. N. Brothers, K. N. Kudin, V. N. Staroverov, T. A. Keith, R. Kobayashi, J. Normand, K. Raghavachari, A. P. Rendell, J. C. Burant, S. S. Iyengar, J. Tomasi, M. Cossi, J. M. Millam, M. Klene, C. Adamo, R. Cammi, J. W. Ochterski, R. L. Martin, K. Morokuma, O. Farkas, J. B. Foresman, D. J. Fox, *Gaussian 16 (version Revision C.01)*, Gaussian, Inc., Wallingford, CT, 2016.
38 J.-D. Chai and M. Head-Gordon, *Phys. Chem. Chem. Phys.*, 2008, **10**, 6615–6620.
39 S. Grimme, *J. Comput. Chem.*, 2006, **27**, 1787–1799.
40 F. Weigend and R. Ahlrichs, *Phys. Chem. Chem. Phys.*, 2005, **7**, 3297–3305.
41 S. Grimme, *J. Chem. Theory Comput.*, 2019, **15**, 2847–2862.
42 P. Pracht, F. Bohle and S. Grimme, *Phys. Chem. Chem. Phys.*, 2020, **22**, 7169–7192.
43 P. Pracht, S. Grimme, C. Bannwarth, F. Bohle, S. Ehlert, G. Feldmann, J. Gorges, M. Müller, T. Neudecker, C. Plett, S. Spicher, P. Steinbach, P. A. Wesołowski and F. Zeller, *J. Chem. Phys.*, 2024, **160**, 114110.
44 S. S. V Sowndarya, P. C. St John and R. S. Paton, *Chem. Sci.*, 2021, **12**, 13158–13166.
45 G. S. Hammond, *J. Am. Chem. Soc.*, 1955, **77**, 334–338.
46 D. S. Hamilton and D. A. Nicewicz, *J. Am. Chem. Soc.*, 2012, **134**, 18577–18580.
47 D. J. Wilger, J.-M. M. Grandjean, T. R. Lammert and D. A. Nicewicz, *Nat. Chem.*, 2014, **6**, 720–726.
48 N. P. R. Onuska, M. E. Schutzbach-Horton, J. L. R. Collazo and D. A. Nicewicz, *Synlett*, 2019, **31**, 55–59.
49 S. Qian, T. M. Lazarus and D. A. Nicewicz, *J. Am. Chem. Soc.*, 2023, **145**, 18247–18252.